Sign in

AMERICAN METEOROLOGICAL SOCIETY
AMS Journals Online

AMS Home | Journals Home | Journal Archive | Subscribe | For Authors | Help | Advanced Search | Search | Go

Full Text View

Volume 32, Issue 3 (March 2002)

Journal of Physical Oceanography
Article: pp. 945–956 | Abstract | PDF (2.16M)

Mixing on a Shallow Shelf of the Black Sea

I. D. Lozovatsky* **and H. J. S. Fernando**

Environmental Fluid Dynamics Program, Department of Mechanical and Aerospace Engineering, Arizona State University, Tempe, Arizona

(Manuscript received March 30, 2001, in final form July 31, 2001)

DOI: 10.1175/1520-0485(2002)032<0945:MOASSO>2.0.CO;2

ABSTRACT

Microstructure measurements were carried out on the shallow shelf of the Black Sea, from the sea surface to the bottom, using a free-falling BAKLAN-S profiler released from an anchored ship. A northeast to southwest transect consisting of eight measurement stations, with several casts made at each station, enabled the evaluation of microstructure statistics across the shelf. The eddy and scalar diffusivities as well as the mixing efficiencies were evaluated for distinct layers that were identified based on mean stratification and the "state" of turbulence. These include five main layers with persistent features (upper and bottom boundary layers, diurnal and main pycnoclines, and a stratified weakly turbulent inner layer) and several transient (patchy) features embedded within such layers (quasi-homogeneous, active turbulent, stratified dissipative, and microstructure displacement patches). The Thorpe displacement scale L_{Th} measurements of this study, together with those reported in Dillon and Gibson et al. indicated that the normalized (by the patch thickness h_p) Thorpe scale L_{Th}/h_p is a function of the mixing Reynolds number R_m and the patch Richardson number Ri_p, but approaches a constant value for high R_m. Layer-averaged diffusivities, which are of direct utility in computing vertical transports at various depths in shelf waters, were evaluated and from which the weighted column-averaged diffusivity $\langle \mathbf{K} \rangle \approx 10^{-4}\ \mathrm{m}^2\ \mathrm{s}^{-1}$ in the Black Sea shallow shelf waters under moderate winds in the beginning of the autumn transition season was estimated. This latter value, however, may be an underestimation given the neglect of near-surface (<3 m) turbulent mixing in the calculations.

Table of Contents:
- Introduction
- Observational program
- Identification of microstructure
- Overturn length scale
- Eddy diffusivities
- Summary
- REFERENCES
- APPENDIX
- TABLES
- FIGURES

Options:
- Create Reference
- Email this Article
- Add to MyArchive
- Search AMS Glossary

Search CrossRef for:
- Articles Citing This Article

Search Google Scholar for:
- I. D. Lozovatsky
- H. J. S. Fernando

1. Introduction

The structure of turbulence in shelf waters differs from that of deep oceans in that turbulence production zones occupy a considerable portion of the water column. Wind mixing and nighttime convection generate turbulence near the sea surface, whereas in the bottom boundary layer enhanced shear (frictional effects) is a major source of turbulence. Storm surges may generate turbulence in both the upper and bottom boundary layers. Sandwiched between these layers is a layer of stratified waters with intermittent (patchy) turbulence produced by breaking internal waves and shear instability. In addition, upwelling circulation, local fronts, coastal jets, barotropic and baroclinic tidal flow, and other flow features influence shelf waters, thus making shelf turbulence a complex phenomenon. Because of the variability of diurnal and seasonal forcing, the shelf water column shows wide variability in space and time. However, certain basic features are persistent and characterize the general turbulence climatology of the shelf. For example, daytime heating and wind-induced turbulence lead to the development of a shallow diurnal pycnocline below the upper mixed layer (Simpson and Hunter 1974). Daytime stratification is eroded and can be destroyed by nocturnal convection (Anis and Moum 1994).

An extensive bibliography is available on small-scale processes on shelves, but most of the reported works are based on CTD profiling and current–temperature moorings (e.g., Kundu 1977; Lentz and Trowbridge 1991). Relatively few publications exist, however, on direct microscale turbulent measurements on shallow shelves. These include the measurements of Dewey et al. (1988) at the shelf of Vancouver Island, Agrawal and Aubrey (1992) at Cape Cod, and Lozovatsky et al. (1999) at the west coast of the Black Sea. Preliminary results of recent extensive microstructure measurements at the shelf of New England were reported by Dillon et al. (1998), Gregg and MacKinnon (1998), and MacKinnon and Gregg (1998). Rehmann and Duda (2000) showed, for example, a sharp decrease of diapycnal diffusivity on the New England shelf with the increase of the density gradient.

A related case is turbulence in shallow seas. For example, measurements in the Baltic Sea by Lozovatsky et al. (1977) and in the Irish Sea by Simpson et al. (1996) show that in shallow waters the turbulent kinetic energy dissipation rate ε generally decreases away from the surface and the bottom toward the interior of the water column. Lozovatsky et al. (1999) reported that the averaged $\langle \log_{10}\varepsilon(z)\rangle$ profile on the Black Sea shelf can be approximated by a parabola, with the lowest turbulent kinetic energy dissipation $\varepsilon_{\min} \approx 5 \times 10^{-10}$ W kg^{-1} occurring at the middepth. This averaged profile, however, represents contributions of a number of individual profiles that contain microstructure features at different stages of evolution. For better understanding, both the averaged and in situ microstructure properties should be studied. Such an attempt will be made in this paper using a set of data rich in microstructure taken from a ship anchored on the Black Sea shelf. The observational region was essentially free of tidal forcing and strongly sheared currents.

Section 2 contains a brief description of the experiment, instrumentation, data processing, and meteorological and hydrological conditions of the study region. Based on the nature of turbulence and stratification, several microstructure layers are identified in section 3. These include five main “persistent” layers and six transient layers. Section 4 presents the dependence of the normalized Thorpe scale in these layers on the turbulent Reynolds and Richardson numbers. Estimates of turbulent diffusivities of each layer and over the entire water column are given in section 5. The summary of the study is presented in section 6.

2. Observational program

a. Experiment

The measurements were carried out on the shallow Black Sea shelf, off the Bulgarian port of Varna on 11 October 1989, as a part of a special microstructure field experiment (Lozovatsky and Ozmidov 1992). A free-fall BAKLAN-S profiler (Paka et al. 1999) was used to measure the vertical structure of temperature, conductivity, and small-scale shear from the sea surface down to the bottom. The data were collected, from a few meters below the sea surface to very near the bottom, at eight stations along a transect approaching the shore from NE to SW; the coastline is approximately in the south–north direction. Station 1 is 8 miles offshore; the distances between first five stations varied from 1.0 to 1.4 miles; the depth of the water column varied from 31 to 25 m. A series of 4–5 casts, with an average time separation of 2–3 minutes, was taken at each of the first five stations. Some of the data from Stations 6 and 7 are unavailable due to instrument malfunction. At the last station (Station 8), located 2.5 miles from the coast with a water depth of 22 m, 12 casts were taken. The measurements were accompanied by routine meteorological observations. An Aandera current meter placed at different depths for short time periods (5 min each) on the lee side of the ship was used to observe background currents. Averaged horizontal components $\bar{u}$ and $\bar{v}$ of the current were used to estimate the mean vertical shear at the time of observation.

b. Instruments and data processing

The BAKLAN-S profiler (a shallow-water version of BAKLAN (Paka et al. 1999) carries an array of sensors consisting of a shear probe, a capillary conductivity probe, and a resistance-wire temperature sensor. The profiler was launched from the windward side of an anchored ship. The cable sank with slack loops slightly slower than the profiler, which minimized the adverse effects of cable movement on measurements. The speed of cable release exceeded the fall speed of the profiler. The sampling rate for each signal was selected in consonance with the time constant and spatial resolution of the corresponding

sensor. Technical information on BAKLAN-S sensors, including the transfer functions, noise level spectra, and accuracy of the measurements, is given in Paka et al. (1999).

Data processing was initiated by eliminating sharp random spikes from the records that may result from plankton contamination. We used three-point initial median filtration. Thereafter, all records were presmoothed by a low-pass cosine filter. A five-point window was used for the conductivity time series and a three-point window was applied to other channels due to the difference in sampling frequencies (260 Hz for conductivity C and 130 Hz for small-scale shear du'/dz and temperature T). This procedure reduced high-frequency electronic noise and gave equally spaced time series of T, C, and du'/dz. Pressure records sampled at 32 Hz were interpolated at the same time intervals as other signals (Δt = 1/130 s). The BAKLAN-S descended at a speed of 0.61 m s^{-1}; thus, the vertical sampling interval dz for all channels was 0.0047 m.

The kinetic energy dissipation rate was computed using the isotropic formula $\varepsilon = 7.5\nu\overline{(du'/dz)^2}$ with 0.2 m vertical averaging, which was used to calculate the eddy mass diffusivity (Oakey 1982),

$$K_N = \gamma\frac{\varepsilon}{N^2}, \qquad (1)$$

where $\gamma = R_f/(1 - R_f)$ is the mixing efficiency, taken as 0.2 for active turbulent patches (Gregg 1987), and R_f is the flux Richardson number. The buoyancy frequency N^2 was computed by Thorpe-ordered density profiles with averaging over the same 0.2-m depth intervals.

The scalar dissipation rate χ_{sc} was calculated using the vertical profiles of conductivity $C(z)$. Traces of conductivity fluctuations $C'(z)$ were obtained by subtracting the linear mean trend of conductivity variations from the conductivity profiles $C(z)$, at each 0.2-m segment. Differentiation of $C'(z)$ and averaging over Δz = 0.2 m give the variance of microconductivity gradient $\overline{(dC'/dz)^2}$. The mean gradient $\overline{\Delta C/\Delta z}$ at each segment was taken as the estimate of the linear trend.

The simplest relationship between the dissipation rates of temperature χ_T and a conductivity χ_{sc} is

$$\chi_T = \chi_{sc}(\partial T/\partial C)^2, \quad (2)$$

where

$$\chi_{sc} = 6D\overline{(dC'/dz)^2}, \qquad (3)$$

and $D \approx 1.4 \times 10^{-7}$ m^2 s^{-1} is the molecular diffusivity of temperature. The ratio $\partial T/\partial C$ is calculated using the temperature coefficient of conductivity

$$\gamma_C = \frac{1}{C_o}\left(\frac{\partial C}{\partial T}\right)_{S_o,T_o},$$

where $C_o(z)$ is the reference conductivity. The ratio $\partial T/\partial C$ of the Black Sea shelf varied in the narrow range of 0.0534–0.0539 S m^{-1} K^{-1}. Washburn et al. (1997), however, have argued that the relationship between χ_{sc} and χ_T can be more intricate than (2) and (3) in that it depends on the T–S correlation in the layer being analyzed, the shape of the conductivity spectrum, the transfer function of the conductivity channel, and several other characteristics.

Since the spatial resolution of the capillary conductivity sensor was limited to $O(0.01)$ m, a correction was applied to the data in the layers being analyzed. The variance loss correction employed was similar to that of Peters et al. (1995), wherein it was assumed that the Batchelor (1959) spectrum is valid at high wavenumbers of the conductivity spectrum, with ε measured using the airfoil probe. The accuracy of this approach, however, can be questioned due to possible nonuniversality of the conductivity spectrum at higher wavenumbers, which is dependent on both temperature and salinity fluctuations. In addition, as pointed out by Miller and Demotakis (1996), the temperature spectrum may not be universal even in the convective–inertial subrange! Detailed analysis of Washburn et al. (1997) shows that the shape of the conductivity spectrum does not seriously affect χ_T if $\chi_T < 10^{-8}$ K^2 s^{-1} and the ratio $\Delta S/\Delta T$ is positive or weakly negative. This condition is satisfied in the present case, where $\Delta S/\Delta T$ varies from −0.05 to −0.02 psu K^{-1}; hence, the influence of the high wavenumber spectral shape on the accuracy of the scalar dissipation measurements is not crucial.

When the conductivity stratification is dominated by the temperature, the scalar diffusivity

$$K_{sc} = \chi_{sc}/2(\overline{\Delta C/\Delta z})^2 \qquad (4)$$

and the conductivity dissipation $K_T = \chi_T/2(\overline{\Delta T/\Delta z})^2$ (Osborn and Cox 1972) can be interchangeably used. As pointed out by Ruddick et al. (1997), γ is related to the scalar dissipation as

$$\gamma = \frac{\chi_T N^2}{2\overline{T}_z^2 \varepsilon}. \qquad (5)$$

We will use the so-called buoyancy Reynolds number

$$\mathrm{Re}_b = \frac{\varepsilon/\nu N^2}{G_{cr}} \qquad (6)$$

in the context of determining the hydrodynamic "state of turbulence" in stratified layers, although several physical meanings have been given to it (Ivey and Imberger 1991). According to Stillinger et al. (1983) and other subsequent work (Ivey and Imberger 1991), when $\varepsilon/\nu N^2 < G_{cr} \approx$ (11–33), all turbulence scales are affected by viscous and buoyancy effects, and hence the turbulence is called fossilized (Gibson 1980). Assigning $\gamma = 0.2$ and $G_{cr} = 30$ as the "canonical" values, $\mathrm{Re}_b = K_N/6\nu$. It can be shown that the mixing Reynolds number, defined as

$$R_m = K_{sc}/\nu, \quad (7)$$

is related to Re_b and γ as $R_m \sim (\gamma \mathrm{Re}_b)^{1/2}$.

c. Meteorological conditions

A mild storm that prevailed over the western coast of the Black Sea before the measurement program appeared to have influenced the microstructure activity. Details of the background hydrophysical and meteorological conditions and their evolution are discussed in Lozovatsky and Ozmidov (1992) and Lozovatsky et al. (1999) and are summarized below. The mean wind stress at the sea surface during the measurement period was $|\tau_a| = 1.34 \times 10^{-2}$ N m^{-2} and the rate of work done by the wind 10 m above the sea surface was $E_{10} = 4 \times 10^{-2}$ W m^{-2}. The surface heat and buoyancy fluxes reversed the sign during the observational period. At 1500 UTC, the total downward heat flux was 125 W m^{-2}, whereas at 1800 UTC the heat flux became −65 W m^{-2}, with the corresponding change of buoyancy flux being -7.3×10^{-8} to 4×10^{-8} W kg^{-1}. The total daytime heat insolation at the sea surface was estimated to be 7 MJ m^{-2}. This stabilizing heat flux, together with mild wind forcing, led to the formation of a shallow upper mixed layer ($z <$ 4–5 m) above the diurnal thermohalocline located at $z \approx$ 5–6 m.

3. Identification of microstructure layers

a. Principal layers

A general view of stratification and corresponding turbulence characteristics along the measurement transect is given in Fig. 1. The contour plots of $\log_{10}N^2$ and $\log_{10}\mathrm{Re}_b(z, x)$ together with the profiles of temperature $T(z)$, salinity $S(z)$, and specific potential density $\sigma_\theta(z)$ taken 20 minutes apart at Station 8 during casts 2 and 12 (Fig. 2) exhibit several prominent features of the thermohaline structure and turbulence on the shelf. These include an upper turbulent layer ($z <$ 4.5 m) with a high dissipation rate ($\varepsilon > 10^{-8}$ W kg^{-1}), a bottom boundary layer ($z >$ 18 m) with strong shear ($\overline{\mathrm{Sh}}^2 > 6 \times 10^{-4}$ s^{-2}), and an intermediate region between the upper and lower boundary layer with patchy turbulence (see, e.g., the region in Fig. 1b with $\mathrm{Re}_b > 100$ in the depth range between 12 and 16 m). A strong narrow thermocline with mean temperature gradient $dT/dz \sim$ 5°C m^{-1} and $N \sim$ 0.15 s^{-1} separated the bottom boundary layer from the water above (Fig. 2). Careful inspection of Figs. 1 and 2 indicates the possibility of classifying the coastal water column to the following distinct layers:

1. The quasi-homogeneous upper turbulent layer (UBL) appearing near the surface, associated with moderate wind stress and daytime heating. UBL is clearly observed at stations 4 and 5 (Fig. 1, regions with $N^2 < 5 \times 10^{-4}$ s^{-2} and $\mathrm{Re}_b > 10$). The measurements taken at these stations in the depth range 3.0–5.2 m were used to estimate turbulent diffusivities for UBL.

2. The bottom boundary layer BBL. The thickest BBL (z = 18.4–23.8 m) was detected at Station 8; see region with $N^2 < 5 \times 10^{-4}$ s^{-2} and $\mathrm{Re}_b > 1$. This station was selected to investigate the mixing activity in the BBL.

3. The main pycnocline layer with intermittent turbulence (ITPC). This refers to the sharp thermohalocline aloft the BBL. Station 5 was chosen to calculate mixing coefficients representative of this layer, which can be seen in the depth range z = 15.8–18.6 m with $N^2 > 10^{-3}$ s^{-2}.

4. The diurnal pycnocline (DPC), which underlies the UBL, resulting from daytime heating and wind stirring. Because of its limited vertical extent, the microstructure samples taken in DPC are insufficient for statistical averaging of turbulent quantities. Therefore, only a little attention was given to this layer.

5. The layer between the DPC and ITPC was usually weakly turbulent and is called the stratified inner layer (SIL). To analyze mixing processes in SIL, the data taken at Stations 2 (z = 8.0–11.0 m) and 8 (z = 11.8–12.6 m) with $N^2 > 5 \times 10^{-4}$ s^{-2} and $\mathrm{Re}_b < 1$ were employed.

b. Secondary layers

The above principal layers were embedded with transient phenomena resulting from the interaction between stratification, shear, and turbulence. For example, strong turbulent zone, such as at Station 3 (Fig. 1) in the depth range $12.2 < z < 16.4$ m, appeared due to strong local internal shear, as evident from the shear estimates given in Fig. 2 (see also Lozovatsky et al., 1999). These regions will be called shear turbulent zones (STZs), and we have utilized data taken at Station 3 to estimate representative turbulent diffusivities of STZs.

Another transient mixing phenomenon, “quasi-homogeneous patches” (QHPs), can be defined as extended regions with $N^2 < 10^{-4}$ s^{-2} and the amplitudes of du'/dz being higher than the background small-scale velocity fluctuations within the SIL. An example of QHP in the depth range from 8.2 to 10.1 m is marked in Fig. 3a, where 12 sequential buoyancy frequency N^2 and kinetic energy dissipation ε data taken at Station 8 are plotted. The mixed nature of QHPs can be attributed to either present or past turbulent events or to the intrusion of mixed water masses into the measurement location. A similar feature was seen at Station 5 over $7.2 < z < 9.2$ m (see Fig. 1).

It should be noted that the time records at Station 8 were taken in the presence of a northward mean current of 10–14 cm s^{-1} in the depth range 6–12 m (Fig. 2), which corresponds to an advection of the water masses over a distance of about 150–200 m during 25 minutes of measurements.

The contours of $\varepsilon(z, t)$ in Fig. 3b show two regions with comparatively high dissipation rates (marked by arrows). The upper high ε patch is signified by $\log_{10}\varepsilon > -8.9$ (W kg^{-1}) in the range $8.1 < z < 9.2$ m and it barely overlapped with QHP. The lower patch, $z > 9.2$ m, was in an area of much higher stratification ($\overline{N} = 2.5 \times 10^{-2}$ s^{-1}), $\log_{10}\varepsilon > -9.0$ (W kg^{-1}), and with time descended into deeper waters. Apparently, the relatively strong small-scale turbulence (high ε) has not acted to destroy the stratification. This stratified region did not contain significant overturning activity, as evident from the rms. Thorpe displacements are shown in Fig. A1. The upper patch with $N^2 < 5 \times 10^{-4}$ s^{-2} and $\varepsilon < 1.25 \times 10^{-9}$ W kg^{-1} will be referred to as the “active patch” (AP) and the lower patch with $\varepsilon > 10^{-9}$ W kg^{-1} but with $1.6 \times 10^{-3} > N^2 > 10^{-4}$ s^{-2} will be called the “stratified dissipative patch” (SDP). The arrows in Fig. 3b mark AP and SDP.

Thorpe displacements are depicted in Fig. 4a for the highly stratified lower part of the pycnocline between 12 and 15 m. There were no inversions in the averaged (over 0.2 m) T, S, C, and σ_θ profiles at these depths, indicating the absence of fluctuations associated with fine-structure interleaving. Note that nonzero Thorpe displacements are mainly confined to depths 12.6–14.6 m, which overlaps the areas of turbulent activity $\mathrm{Re}_b > 1$ or $\varepsilon/\nu N^2 > 30$. This region will be called the “microstructure displacement patch” (MDP).

4. Overturn length scale in patches

The Thorpe (overturning) scale L_{Th} (Thorpe 1977) is used to characterize the sizes of turbulent eddies. Laboratory experiments and field studies reported hitherto show that the normalized Thorpe scale L_{Th}/h_p varies in a wide range, where h_p is the thickness of mixed regions. If the breakdown of turbulent eddies transfers kinetic energy down the cascade, the probability distribution function $F(L_{Th}/h_p)$ is expected to be log-normal, because Kolmogorov's (1941) theory postulates that the sizes of particles resulting from a series of successive statistically independent breaking must be asymptotically log-normal.

The present data were used to evaluate the Thorpe scale L_{Th} and the thickness of mixed regions h_p (see the appendix for details). Figure 5 shows the probability distribution function $F(L_{Th}/h_p)$ of normalized Thorpe scale L_{Th}/h_p in several oceanic environments. The data include the present measurements and those obtained in the North Pacific at Ocean Weather Station P (Dillon 1982, Tables 1 and 2) and near Ampere Seamount in the eastern subtropical Atlantic (Gibson et al. 1993, Table 2). The straight lines represent log-normal approximations, which show that the ensuing probability distributions are reasonably well described by the log-normal model. The arrows placed along the horizontal axis in Fig. 5 show the median values of L_{Th}/h_p for AP, QHP, and MDP of the present work and for those reported by Dillon (1982), Gibson et al. (1993), and Peters et al. (1995). The range of L_{Th}/h_p obtained by De Silva and Fernando (1992) in laboratory experiments with continually forced turbulent patches is shown by the horizontal arrow. The variability of the median values over more than one decade, from 0.027 to 0.35, suggests that the normalized length scales L_{Th}/h_p are dependent on the "state of evolution" of the patch, which can be specified by the nondimensional parameters that signify the nature of turbulence and stratification.

To further investigate L_{Th}/h_p variability, it is possible to invoke the relationships between internal parameters of stratified turbulence and external parameters such as the mixing Reynolds number $R_m = K_{sc}/\nu$ and the patch Richardson number $\mathrm{Ri}_p = N^2 h_p^4/K^2$ (see the appendix for details). An increase of stratification (growing Ri_p) should lead to a decrease of L_{Th}/h_p, while an increase of mixing (growing R_m) may yield higher L_{Th}/h_p. The data of the present study along with those of Dillon (1982) and Gibson et al. (1993) were analyzed to delineate the dependence of L_{Th}/h_p on R_m and Ri_p. It was found that the nondimensional function P^*,

$$\hat{L}_{Th} \equiv \frac{L_{Th}}{h_p} = P^*\left[\frac{0.3}{(1 + \mathrm{Ri}_p/60)^{1/4}(1 + 150/R_m)}\right] = P^*(x), \quad (8)$$

correlates well with L_{Th}/h_p data (Fig. 6) (see the appendix). A least squares linear approximation of the nondimensional function (8) in the form of $P^* = 0.03 + 1.5x$ and the coefficient of determination $r^2 = 0.89$ explains more than 80% of the variance of the normalized Thorpe scales observed in stratified regions of diverse properties. It appears that the parameterization (8) is valid for several oceanic regions, and further tests are necessary to evaluate its universality.

Peters et al. (1995) argued that, when the mixing region does not embrace a segment of the Thorpe displacement profile with prominent double maxima (e.g., a turbulent patch within a homogeneous layer), the thickness h_p might not be uniquely identified. Accordingly, calculations of h_p for AP and QHP (15% of all data used in this section) were based on an alternative approach that relies on the definitions of microstructure regions given in section 3. Samples of L_{Th}/h_p of these patches, therefore, may not be treated with the same confidence as those of MDP and the data of Dillon (1982) and Gibson et al. (1993).

5. Eddy diffusivities

In section 3, five main (seasonal) layers and several transient regions of the water column were identified, and the vertical transport on the shelf is expected to be influenced by all these layers. We calculated the bootstrap (Efron 1982) estimates of the mean for the mass $\hat{K}_N$ and scalar $\hat{K}_{sc}$ diffusivities of every region. The results are shown in Table 1 (along with 90% confidence limits) and in Fig. 7a. The bootstrap samples used for domain averaging were ten times the actual number of samples available for each region (Table 1). Figure 7a indicates that $\hat{K}_{sc}$ and $\hat{K}_N$ are linearly dependent, at least for $K > 5 \times 10^{-6}$ m^2 s^{-1} as

$$\hat{K}_{sc} = \hat{K}_N, \quad (10)$$

with a coefficient of determination 0.96. A plot of domain-averaged mixing efficiency $\hat{\gamma}$ calculated based on (5) as a function of the buoyancy Reynolds number $\hat{\mathrm{Re}}_b$ is shown in Fig. 7b. The mixing efficiency becomes independent of Re_b as Re_b grows for properly clustered averaged samples. It appears that $\hat{\gamma} \approx 0.2$ for actively turbulent regions with $\hat{\mathrm{Re}}_b > 1$.

In weakly turbulent stratified layers (e.g., SIL), $\hat{K}_{sc}$ is about one order of magnitude larger than $\hat{K}_N$—the latter being about twice the molecular diffusivity, perhaps due to prevailing fully fossilized turbulence as a result of $\hat{\mathrm{Re}}_b < 1$. Under these conditions, the assumptions of local isotropy (used to evaluate ε and χ_{sc}) and stationarity of kinetic energy and scalar variance [used to derive (1) and (4)] are highly questionable, and $\hat{\gamma}$ so derived should be viewed with caution.

Finally, it is instructive to estimate the overall eddy coefficients in the shelf waters of the Black Sea at the end of summer heating based on volume-averaged diffusivities of each of the principal and transient regions identified in section 3. The measured diffusivities can be cast in terms of a "canonical" value for the deep ocean pycnocline, $K_o = 10^{-5}$ m^2 s^{-1} (Gregg 1987; Ledwell et al. 1993), and the results are as follows.

(i) In the UBL, under mild winds, the diffusivity is about $40K_o$.

(ii) The stratified BBL influenced by near-bottom current shows a diffusivity close to $3K_o$.

(iii) In active turbulent regions inside the water column (QHP, STZ), the diffusivity lies between $2K_o$ and $15K_o$.

(iv) In strongly stratified pycnoclines with intermittently generated turbulence (ITPC, DPC), the diffusivity is in the range $0.2K_o$–$0.3K_o$.

The layers (i), (ii), (iii), and (iv) occupy approximately 20%, 25%, 15%, and 10%, respectively, of the total depth range; the rest of the water column is occupied by almost nonturbulent ($K < 0.1K_o$) stratified waters. If the above estimates are representative of typical background hydrological and meteorological conditions at the end of the summer season in the northern part of the Black Sea, a rough estimate of the weighted average vertical diffusivity over a unit area of the shelf can be obtained as $\langle K \rangle = (9–11)K_o$. This estimate of $\langle K \rangle$ is close to Munk's (1966) estimate for the main oceanic pycnocline based on global energetics. It is also of interest that $K_N \approx 10^{-4}$ m^2 s^{-1} was measured recently by MacKinnon and Gregg (1998) on the tidally affected continental shelf of New England during the passage of high-amplitude internal waves. In the present case, the overall shelf diffusivity $\sim 10^{-4}$ m^2 s^{-1} is mainly contributed by sustained turbulence in the boundary layers, which occupy a substantial portion of the shallow water column. It should be noted that the near-surface (0–3 m) layer contaminated by boat motion was not considered in this analysis. Therefore, the calculated value $\langle K \rangle \approx 10^{-4}$ m^2 s^{-1} is probably an underestimation of the column-averaged vertical diffusivity under given background conditions.

6. Summary

The aim of this paper was to estimate eddy diffusivities and variables characterizing turbulent mixing on the shallow (depth <30 m) shelf of the Black Sea near the Bulgarian coast. Of particular interest was to identify major microstructure layers (features) of different states of evolution and to study the turbulent scales (e.g., Thorpe scales) within them. Vertical profiles of temperature, conductivity and small-scale shear were measured over the entire water column over a NW to SE transect across the shelf using free-falling microstructure profiler BAKLAN-S. *Five principal hydrodynamic layers* [the upper and bottom boundary layers (UBL and BBL), separated by a weakly turbulent inner stratified layer (SIL), and sharp diurnal and main pycnoclines (DPC and ITPC)], and *five transient (secondary) microstructure features* [active (AP), quasi-homogeneous (QHP), and stratified dissipative (SDP) turbulent patches, shear turbulent zone (STZ), and microstructure displacement patch (MDP)] embedded in the principal layers were identified. The delineation of these layers was based on the buoyancy frequency N, dissipation rate of the turbulent kinetic energy ε, buoyancy Reynolds number $\mathrm{Re}_b = \varepsilon/30\nu N^2$, and the Thorpe displacements d'.

The measurements were used to calculate such quantities as the mass diffusivity K_N, scalar diffusivity K_{sc}, the mixing

efficiency γ, the patch thickness h_p, as well as the Thorpe length scale L_{Th}. The ratio L_{Th}/h_p was found to depend on background conditions, and its probability distribution function was log-normal for QHP, AP, and MDP. The median values of L_{Th}/h_p distributions varied over a decade from 0.027 to 0.35 depending on the state of turbulence (mixing Reynolds number, $R_m = K_{\mathrm{sc}}/\nu$) and stratification (patch Richardson number, $Ri_p = N^2 h^4_p/K^2_{\mathrm{sc}}$). Higher values of L_{Th}/h_p were associated with regions of active, fully developed turbulence.

On dimensional grounds, L_{Th}/h_p was proposed to be a function of R_m and Ri_p. The present observations along with those of Dillon (1982) and Gibson et al. (1993) confirmed this proposal and showed that L_{Th}/h_p is an increasing function of R_m when $R_m < 150$ and a constant ($L_{\mathrm{Th}}/h_p \sim 0.3$) for $R_m > 150$. For a constant R_m, L_{Th}/h_p decreased with Ri_p.

It was also shown that the correlation between eddy and scalar diffusivities K_N and K_{sc} strongly depends on space–time averaging. For domain-averaged diffusivities (bootstrap estimates), the results showed that $\hat{K}_{\mathrm{sc}} \approx \hat{K}_N$ for $\hat{K} \geq 10^{-5}$ m^2 s^{-1}, with a mixing efficiency of $\hat{\gamma} \approx 0.2$. In highly stratified layers with weak turbulence, $\hat{K}_{\mathrm{sc}} > \hat{K}_N$ and $\hat{\gamma}$ grows to 0.5–0.6. The domain-averaged diffusivities vary in the range (0.4–4.0) × 10^{-4} m^2 s^{-1} in the bottom and surface boundary layers and shear turbulent zone. In sharp pycnoclines, it assumes values of (1–2) × 10^{-6} m^2 s^{-1}.

Based on these representative values of $\hat{K}$ in various layers, an overall water column–averaged vertical eddy diffusivity on the shelf was evaluated as ‹K› = (9–11) × 10^{-5} m^2 s^{-1}. Despite the lack of data in the upper 3 m of the water column (about 10% of the total shelf depth), the above value can be used to characterize overall mixing on the shallow shelf of the Black Sea in the beginning of autumn where winds are moderate and multilayered density stratification is well established. Nevertheless, significant variation of $\hat{K}$ with depth shows that the column-averaged diffusivity ‹K› is not an appropriate measure for the computation of vertical transports through the thermocline. The depth-dependent, layer-averaged diffusivities $\hat{K}$ rather than ‹K› should be used for computation of vertical transports in shelf waters.

Acknowledgments

The field measurements were carried out as a part of an international coastal experiment Varna-89, which was funded by the Bulgarian and Russian Academies of Sciences. We are indebted to Valeri Nabatov and Anatoli Erofeev who headed observational and data processing teams during the experiment. The analysis was performed under Grant N00014-97-1-0140 of the U.S. Office of Naval Research.

REFERENCES

Agrawal Y. C., and D. G. Aubrey, 1992: Velocity observations above a rippled bed using laser Doppler velocimetry. *J. Geophys. Res.*, **97**, 20249–20259. Find this article online

Anis A., and J. N. Moum, 1994: Prescriptions for heat flux and entrainment rates in the upper ocean during convection. *J. Phys. Oceanogr.*, **24**, 2142–2155. Find this article online

Batchelor G. K., 1959: Small-scale variations of convected quantities like temperature in turbulent fluid: General discussion and the case of small conductivity. *J. Fluid Mech.*, **5**, 113–133. Find this article online

De Silva I. P. D., and H. J. S. Fernando, 1992: Some aspects of mixing in a stratified turbulent patch. *J. Fluid Mech.*, **240**, 601–625. Find this article online

Dewey R. K., P. H. Leblond, and W. R. Crawford, 1988: The turbulent bottom boundary layer and its influence on local dynamics over the continental shelf. *Dyn. Atmos. Oceans*, **12**, 143–172. Find this article online

Dillon T. M., 1982: Vertical overturns: A comparison of Thorpe and Ozmidov length scales. *J. Geophys. Res.*, **87**, 9601–9613. Find this article online

Dillon T. M., and D. R. Caldwell, 1980: The Batchelor spectrum and dissipation in the upper ocean. *J. Geophys. Res.*, **85**, 1910–1916. Find this article online

Dillon T. M., J. A. Barth, A. Yu. Erofeev, and G. H. May, 1998: Towed observations of scalar dissipation on the mid Atlantic shelf. *Eos, Trans. Amer. Geophys. Union*, **79**(1), 101, OS. Find this article online

Efron B., 1982: *The Jackknife, the Bootstrap and Other Resampling Plans*. *Society for Industrial and Applied Mathematics*, 92 pp.

Gibson C. H., 1980: Fossil temperature, salinity and vorticity turbulence in the ocean. *Mar. Turbul.*, J. C. J. Nihoul, Ed., Elsevier, 221–257.

Gibson C. H., V. N. Nabatov, and R. V. Ozmidov, 1993: Measurements of turbulence and fossil turbulence near Ampere seamount. *Dyn. Atmos. Oceans*, **19**, 175–204. Find this article online

Gregg M. C., 1987: Diapycnal mixing in the thermocline. *J. Geophys. Res*, **92**, 5249–5286. Find this article online

Gregg M. C., and J. A. MacKinnon, 1998: Mixing on a continental shelf during CMO 97—Preliminary results. *Eos, Trans. Amer. Geophys. Union*, **79**(1), 100, OS. Find this article online

Ivey G., and J. Imberger, 1991: On the nature of turbulence in a stratified fluid. Part 1: The energetics of mixing. *J. Phys. Oceanogr.*, **21**, 650–658. Find this article online

Kolmogorov A. N., 1941: On log-normal distribution of the sizes of particle in the course of breakdown (in Russian). *Doklady USSR Akad. Sci.*, **31**((2),), 99–101.

Ledwell J. R., A. J. Watson, and C. S. Law, 1993: Evidence for slow mixing across the pycnocline from an open-ocean tracer-released experiment. *Nature*, **364**, 701–703. Find this article online

Lozovatsky I. D., and R. V. Ozmidov, Eds., 1992: *The Variability of the Hydrophysical Fields in the Coastal Zone during Autumn Cooling*. Vol. 5, *Data of Oceanography Study*, Geophysical Commit., 212 pp.

Lozovatsky I. D., R. V. Ozmidov, and J. C. J. Nihoul, 1977: Bottom turbulence in stratified enclosed seas. *Bottom Turbulence*, J. C. J. Nihoul, Ed., Elsevier, 49–58.

Lozovatsky I. D., T. M. Dillon, A. Yu. Erofeev, and V. N. Nabatov, 1999: Variations of thermohaline and turbulent structure on the shallow Black Sea shelf in the beginning of autumn cooling. *J. Mar. Syst.*, **21**, 255–282. Find this article online

MacKinnon J. A., and M. C. Gregg, 1998: Mechanisms of mixing on the New England continental shelf during CMO 96. *Eos, Trans. Amer. Geophys. Union*, **79**(1), 100, OS. Find this article online

Miller P. L., and P. E. Demotakis, 1996: Measurements of scalar power spectra in high Schmidt number turbulent jets. *J. Fluid Mech.*, **308**, 129–146. Find this article online

Munk W. H., 1966: Abyssal recipes. *Deep-Sea Res.*, **13**, 207–230. Find this article online

Oakey N. S., 1982: Determination of the rate of dissipation of turbulent energy from simultaneous temperature and velocity shear microstructure measurements. *J. Phys. Oceanogr.*, **12**, 256–271. Find this article online

Osborn T. R., and C. S. Cox, 1972: Oceanic fine structure. *Geophys. Fluid Dyn.*, **3**, 321–345. Find this article online

Paka V. T., V. N. Nabatov, I. D. Lozovatsky, and T. M. Dillon, 1999: Ocean microstructure measurements by BAKLAN and GRIF. *J. Atmos. Oceanic Technol.*, **16**, 1519–1532. Find this article online

Peters H. M., M. C. Gregg, and T. B. Sanford, 1995: Detail and scaling of turbulent overturns in the Pacific Equatorial Undercurrent. *J. Geophys. Res.*, **100**, 18349–18368. Find this article online

Rehmann C. R., and T. F. Duda, 2000: Diapycnal diffusivity inferred from scalar microstructure measurements near the New England shelf/slope front. *J. Phys. Oceanogr.*, **30**, 1354–1371. Find this article online

Ruddick B., D. Walsh, and N. Oakey, 1997: Variations in apparent mixing efficiency in the North Atlantic Central Water. *J. Phys. Oceanogr.*, **27**, 2589–2605. Find this article online

Seim H. E., and M. C. Gregg, 1994: Detailed observations of a naturally occurring shear instability. *J. Geophys. Res.*, **99**, 10049–10073. Find this article online

Simpson J. H., W. R. Crawford, T. R. Rippeth, A. R. Campbel, and J. V. S. Cheok, 1996: The vertical structure of turbulent dissipation in shelf seas. *J. Phys. Oceanogr.*, **26**, 1579–1590. Find this article online

Simpson J. J., and J. R. Hunter, 1974: Fronts in the Irish Sea. *Nature*, **250**, 404–406. Find this article online

Stillinger D. C., K. N. Helland, and C. W. Van Atta, 1983: Experiments on the transition of homogeneous turbulence to internal waves in a stratified fluid. *J. Fluid Mech.*, **131**, 91–122. Find this article online

Thorpe S. A., 1977: Turbulence and mixing in a Scottish Loch. *Philos. Trans. Roy. Soc. London*, **A286**, 125–181.

Washburn L., T. F. Duda, and D. C. Jacobs, 1997: Interpreting conductivity microstructure: Estimating the temperature variance dissipation rate. *J. Atmos. Oceanic Technol.*, **13**, 1166–1188. Find this article online

APPENDIX

7. Overturning Scale

a. Calculations

The overturning length scale is usually calculated by reordering a density profile containing inversions to obtain a stable profile with monotonic variation of density. The displacements of fluid parcels d'_i required to do so, known as the Thorpe displacements (Thorpe 1977), are used to estimate the Thorpe scale $L_{\mathrm{Th}} = (\overline{d'^2_i})^{1/2}$, considered as a measure of the typical size of energy-containing eddies producing internal vertical mixing in a stratified fluid.

In calculating oceanic Thorpe displacements, the reordering should be applied to the potential density $\rho_\theta(z)$ profile. The bane of this task is the insufficient vertical resolution of measurements (Peters et al. 1995); for example, the smallest scalar fluctuations are on the order of the Batchelor scale $L_B = c_B(\nu D^2/\varepsilon)^{1/4}$ (i.e., the scale of the maximum temperature gradient) and are hard to resolve. Here, $c_B = 2\pi(2q)^{1/2} \approx 16.5$ for $q = 2(3)^{1/2}$ (Dillon and Caldwell 1980). In calculating d'_i, it has been customary to use instantaneous temperature profiles with the assumption that the correlation between temperature and density is high (Dillon 1982). For temperature fluctuations and $\varepsilon < 10^{-7}$ W kg^{-1}, L_B is of the order of 1 cm, which cannot be resolved by a BAKLAN-S temperature sensor. On the other hand, the microcapillary conductivity probe of BAKLAN-S has much better space resolution ($\sim$ 1 cm: Paka et al. 1999), and hence conductivity measurements could be used to calculate $d'_i(z)$. Figure A1 shows an example of the increased Thorpe displacements $d'(z)$ and $\varepsilon(z)$ in the same depth interval of 8.4–8.7 m, indicating how Thorpe displacements based on conductivity microstructure profiles correlate well with active turbulent layers signified by enhanced ε. In this case, the layer thickness h_p could be determined using Dillon's (1982) approach, $h_p = z_l - z_u$, where z_u and z_l are the upper and lower boundaries of a region wherein $\Sigma\, d'_i = 0$ (see also Seim and Gregg 1994 and Peters et al. 1995). De Silva and Fernando (1992) defined the patch thickness as the minimum distance between the points beyond which $|d'_i| < 0.05\, L^{\max}_{\mathrm{Th}}$, where $L^{\max}_{\mathrm{Th}}$ is the absolute value of the maximum Thorpe displacement. A similar definition was used by Gibson et al. (1993). Because positive and negative $L^{\max}_{\mathrm{Th}}$ are distinct at the edges of patches (see Fig. A1), h_p estimates obtained from these two approaches yield essentially the same h_p.

b. Parameterization

The energy input to the coastal oceans can be considered as sustained, but the events distributed within are evolving and time dependent. If the energy input to a stratified turbulent patch can be specified by the rms velocity σ_u and the integral length scale l and if the patch is generated at time $t = 0$, then any dependent property P in the patch can be written in terms of the governing parameters as

$$P = P_1(\sigma_u, l, N_o, t, \nu), \quad \text{(A1)}$$

where $P_1, P_2, \ldots$ are functions. Since the instantaneous stratification in the patch N is a function of the same independent parameters, it is possible to eliminate t to obtain the nondimensional form

$$P^* = P_2^*\left(\frac{\sigma_u l}{\nu}, \frac{N}{N_o}, \frac{N^2 l^2}{\sigma_u^2}\right). \quad \text{(A2)}$$

Instead of σ_u or l, an eddy viscosity $K_M \sim \sigma_u l$ can be used to parameterize turbulence, namely,

$$P^* = P_3^*\left(\frac{K}{\nu}, \frac{N}{N_o}, \frac{N^2 l^4}{K^2}\right). \qquad \text{(A3)}$$

Using (A3) and assuming that the length scale l is proportional to the patch size h_p and K_{sc} represents turbulent diffusivity, it is possible to write

$$\frac{L_{Th}}{h_p} = P_4^*\left(R_m, \mathrm{Ri}_p, \frac{N}{N_o}\right), \qquad \text{(A4)}$$

or at large times of evolution, wherein $N/N_0 \rightarrow 0$ in a patch but with finite Ri_p (due to large l),

$$\frac{L_{Th}}{h_p} = P_5^*(R_m, \mathrm{Ri}_p). \qquad \text{(A5)}$$

Here $R_m = K_{sc}/\nu$ is the mixing Reynolds number and $\mathrm{Ri}_p = N^2 h^4{}_p/K^2$ is the patch Richardson number.

In comparing data with (A5), a plot of L_{Th}/h_p versus R_m was prepared (Fig. A2a) using the present data and those from Dillon (1982, Table 2) and Gibson et al. (1993). The data covered four orders of magnitude of R_m. Despite the wide scatter of individual samples, some interesting trends could be observed. Up to about R_m = 100–200, L_{Th}/h_p increases linearly with R_m, but at large R_m(>150), L_{Th}/h_p slowly approaches an asymptotic value of about 0.3, and the formula

$$\frac{L_{Th}}{h_p} = \frac{\hat{L}^{\max}_{Th}}{1 + R_{cr}/R_m} \qquad \text{(A6)}$$

was introduced as an approximation for the data (solid line in Fig. A2a) with $\hat{L}^{\max}_{Th} = 0.3$ and $R_{cr} = 150$. The scatter of the data, which leads to a quite low coefficient of determination, $r^2 = 0.47$, suggests the necessity of investigating the sensitivity of L_{Th}/h_p to Ri_p. Several datasets located in narrow R_m ranges were selected from the high R_m regime (to eliminate the R_m effects), and a dependence of normalized Thorpe scale versus square root of the patch Richardson number was plotted in Fig. A2b, where a decrease of L_{Th}/h_p with increasing Ri_p was evident. A least squares power fit to the data gives $L_{Th}/h_p \sim \mathrm{Ri}^{-1/4}{}_p$ (a thin line in Fig. A2b for $\mathrm{Ri}_p > 60$). The 90% confidence limit of the exponent is ±0.05. For $\mathrm{Ri}_p \ll \mathrm{Ri}_o \approx 60$, the normalized Thorpe scale approaches $\hat{L}^{\max}_{Th}$ when $\mathrm{Ri}_p \rightarrow 0$. Considering these asymptotic behaviors at low and high Ri_p, it is possible to introduce the interpolation formula

$$\frac{L_{Th}}{h_p} = \frac{0.3}{(1 + \mathrm{Ri}_p/60)^{1/4}}, \qquad \text{(A7)}$$

which shows the best fit to the data in Fig. A2b. Without knowing the effects of N/N_o, it is not possible to determine the exact dependence of L_{Th}/h_p on the governing parameters, but the results do indicate dependencies of L_{Th}/h_p on R_m for $R_m < 150$ and on Ri_p for $\mathrm{Ri}_p > 60$.

Tables

TABLE 1. The bootstrap estimates of the domain-averaged eddy diffusivities K_N and K_{sc}

Layer name/ station number(s)	Depth range (m)	$\bar{K}_\rho \times 10^4$ ($m^2\ s^{-1}$)	90% confidence intervals for $\bar{K}_\rho \times 10^4$ ($m^2\ s^{-1}$)	Number of samples	$\bar{K}_z \times 10^4$ ($m^2\ s^{-1}$)	90% confidence intervals for $\bar{K}_z \times 10^4$ ($m^2\ s^{-1}$)
UBL/4, 5	3.0–5.2	4.05	2.60–6.04	76	3.82	2.74–5.02
SIL/2	8.0–11.0	0.0038	0.0021–0.0057	73	0.045	0.032–0.058
QHP/8	8.2–10.2	0.19	0.11–0.28	47	0.18	0.14–0.23
QHL/5	7.2–9.2	0.37	0.25–050	33	0.50	0.22–0.83
STZ/3	12.2–16.4	1.35	0.92–1.82	92	1.75	1.26–2.32
ITPC/5	15.8–18.6	0.031	0.02–0.043	55	0.015	0.014–0.016
BBL/8	18.2–23.8	0.33	0.25–0.41	176	0.23	0.20–0.29

Click on thumbnail for full-sized image.

Figures

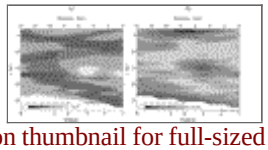

Click on thumbnail for full-sized image.

FIG. 1. Vertical cross sections of (a) $\log_{10} N^2(z, x)$ and (b) $\log_{10} \mathrm{Re}_b(z, x)$, across the shelf; N is in rad s^{-1}. The distances x are counted from Station 1, which was taken about 8 miles off shore. Instruments failed at Stations 6 and 7

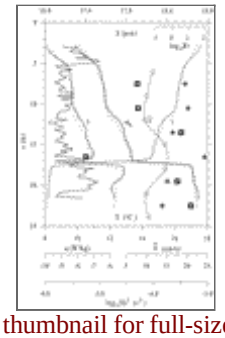

Click on thumbnail for full-sized image.

FIG. 2. Temperature $T(z)$, salinity $S(z)$, and specific potential density $\sigma_\theta(z)$ for casts 2 (solid lines) and 12 (dashed lines) at Station 8. The line with circles shows the modules of the mean currents averaged during the observation period. The squares are the estimates of vertical shear $\log_{10} \mathrm{Sh}^2$ at 3-m segments, and the crosses are the corresponding logarithms of the gradient Richardson number. The turbulent kinetic energy dissipation rate $\mathcal{E}(z)$ (cast 2) shows high turbulence activity in the diurnal pycnocline and in the bottom boundary layer

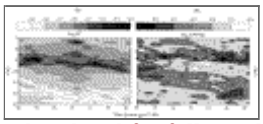

Click on thumbnail for full-sized image.

FIG. 3. Vertical sections of the logarithms of (a) squared buoyancy frequency and (b) the kinetic energy dissipation rate obtained during 12 casts at Station 8. The arrows show the regions that belong to quasi-homogeneous (QHP), active (AP), and stratified dissipative (SDP) patches

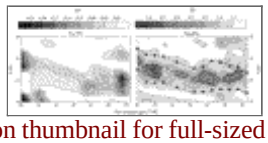

Click on thumbnail for full-sized image.

FIG. 4. Vertical sections of the contours of rms Thorpe displacements (a) and logarithm of the buoyancy Reynolds number (b) in the depth range of MDP. In (b), lines with squares mark the boundaries of MDP. Regions where $\mathcal{E}/\nu N^2 > 30$ are confined by heavy lines and those where $\mathcal{E}/\nu N^2 > 15$ by dashed lines. The latter was included to indicate the sensitivity of the boundary of the turbulent region to the criteria used to determine turbulence

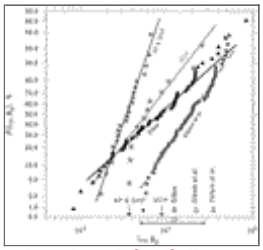

Click on thumbnail for full-sized image.

FIG. 5. Cumulative distribution functions of the normalized Thorpe scales for the samples representing AP and QHP (snow flakes) and MDP (stars). The functions $F(L_{\mathrm{Th}}/h_p)$ shown by triangles and dots were calculated using data from Dillon (1982, Tables 1 and 2) and Gibson et al. (1993, Table 2) respectively. The Kolmogorov–Smirnov test cannot reject the null hypothesis of log-normality at a significance level, which is higher than the standard 5%–10%, unless we use the estimated rather than assumed to be known parameters of the distributions. The bootstrap estimates of the mean normalized Thorpe scale for different datasets, along with the equatorial measurements of Peters et al. (1995), are shown by the arrows along the horizontal axis. Laboratory measurements of L_{Th}/h_p obtained by De Silva and Fernando (1992) (DF) are in the range marked by the horizontal arrows

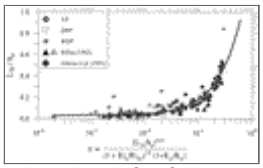

Click on thumbnail for full-sized image.

FIG. 6. The composite plot showing the dependence of the normalized Thorpe scale on the patch Richardson Ri_p and mixing Reynolds R_m numbers according to (8). The curve shows a linear least squares fit to the data

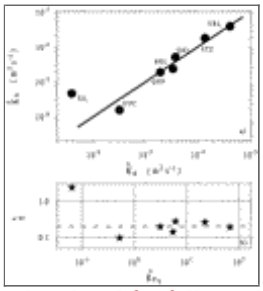

Click on thumbnail for full-sized image.

FIG. 7. (a) Relationship between the averaged eddy mass diffusivity $\hat{K}_N$ and scalar turbulent diffusivity $\hat{K}_{\mathrm{sc}}$ on the shelf, calculated for some representative regions (see Table 1). The straight line is a linear regression $\hat{K}_{\mathrm{sc}} = \hat{K}_N$. (b) Mixing efficiencies $\hat{\gamma}$ vs the buoyancy Reynolds numbers $\hat{\mathrm{Re}}_b$, taken from the same regions; dashed line represents $\hat{\gamma} = 0.2$

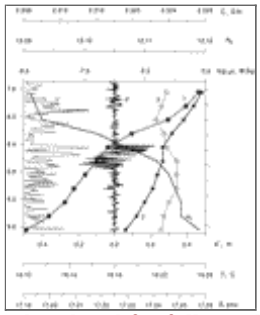

Click on thumbnail for full-sized image.

FIG. A1. The profiles of Thorpe displacements $d'(z)$, local dissipation rate $\varepsilon'(z)$, and mean profiles of temperature (T), salinity (S), conductivity (C), and specific density (σ_θ) for cast 7 at Station 8. Note that the conductivity and density profiles are monotonic; thus, the Thorpe displacements are associated with vertical turbulent mixing rather than fine-scale interleaving. Enhanced $d'(z)$ between 7.7 and 7.8 m and in the 8.4–8.7 depth intervals reflect an increase of local turbulent dissipation

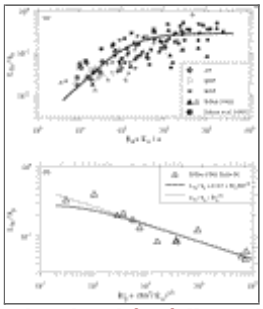

Click on thumbnail for full-sized image.

FIG. A2. The dependence of the normalized Thorpe scale L_{Th}/h_p on the mixing Reynolds number R_m (a) and on the patch Richardson numbers Ri_p (b). The solid line in (a) is the approximation given by (A6)

Corresponding author address: Dr. I. D. Lozovatsky, Environmental Fluid Dynamics Program, Dept. of Mechanical and Aerospace Engineering, Arizona State University, Box 879809, Tempe, AZ 85287. E-mail: i.lozovatsky@asu.edu

* Additional affiliation: P. P. Shirshov Institute of Oceanology, Russian Academy of Sciences, Moscow, Russia

top

© 2008 American Meteorological Society Privacy Policy and Disclaimer
Headquarters: 45 Beacon Street Boston, MA 02108-3693
DC Office: 1120 G Street, NW, Suite 800 Washington DC, 20005-3826
amsinfo@ametsoc.org Phone: 617-227-2425 Fax: 617-742-8718
Allen Press, Inc. assists in the online publication of *AMS* journals.